Published in final edited form as:
*JACC Cardiovasc Imaging*. 2009 May ; 2(5): 637–647. doi:10.1016/j.jcmg.2008.08.009.

# Macrophage-Specific Lipid-Based Nanoparticles Improve MRI Detection and Characterization of Human Atherosclerosis

**Michael J. Lipinski, MD**[1,2,3,4,5], **Juan C. Frias, PhD**[1,2,6], **Vardan Amirbekian, MD**[1,2,7], **Karen C. Briley-Saebo, PhD**[1,2], **Venkatesh Mani, PhD**[1,2], **Daniel Samber, PE**[1,2], **Antonio Abbate, MD**[4], **Juan Gilberto S. Aguinaldo, MD**[1,2], **Davis Massey, DDS, MD, PhD**[8], **Valentin Fuster, MD, PhD**[3], **George W. Vetrovec, MD**[4], and **Zahi A. Fayad, PhD**[1,2,3]

[1]Translational and Molecular Imaging Institute, Mount Sinai Medical Center, New York, NY, USA

[2]Imaging Science Laboratories. Department of Radiology, Mount Sinai Medical Center, New York, NY, USA

[3]The Zena and Michael A. Wiener Cardiovascular Institute. The Marie-Josée and Henry R. Kravis Cardiovascular Health Center. Department of Internal Medicine, Division of Cardiology, Mount Sinai Medical Center, New York, NY, USA

[4]Division of Cardiology, Virginia Commonwealth University, Richmond, VA, USA

[5]Department of Internal Medicine, University of Virginia Health System, Charlottesville, VA, USA

[6]Instituto de Ciencia Molecular, University of Valencia. Valencia, Spain

[7]Department of Radiology, Brigham and Womens Hospital. Boston, MA, USA

[8]Department of Pathology. Virginia Commonwealth University Health System, Richmond, VA, USA

## Abstract

**Objectives—**We sought to determine if gadolinium (Gd)-containing lipid-based nanoparticles (NPs) targeting the macrophage scavenger receptor-B (CD36) improve magnetic resonance (MR) detection and characterization of human atherosclerosis.

**Background—**The ability to detect atherosclerosis with MR imaging using gadolinium Gd-containing lipid-based NPs targeting macrophages may enable early detection of high-risk lesions prior to an atherothrombotic event. Gd-containing lipid-based NPs targeting macrophages improved MR detection of murine atherosclerosis.

**Methods—**Gd-containing NPs, anti-CD36 NPs and Fc-NPs were created. Macrophages were incubated with fluorescent targeted and non-targeted NPs to determine uptake via confocal microscopy and inductively coupled plasma mass spectroscopy (ICP-MS) quatified Gd uptake. Human aortic specimens were harvested at autopsy. Using a 1.5 T scanner, T1, T2, and PDW 3-dimensional scans were performed along with post-contrast scans after 24 h incubation. T1 and cluster analysis were performed and compared with immunohistopathology.



**Corresponding Author**: Zahi A. Fayad, PhD, FAHA, FACC Mount Sinai School of Medicine One Gustave L. Levy Place Imaging Science Laboratories Box 1234 New York, NY 10029 Fax: 212-534-2683 Telephone: 212-241-6858 zahi.fayad@mssm.edu.

**Results—**The NPs had a mean diameter of 125 nm, 14,900 Gd-ions, and relaxivity was 37 $mM^{-1}s^{-1}$ at 1.5T and 37°C. Confocal microscopy and ICP-MS demonstrated significant in vitro macrophage uptake of targeted NPs while non-targeted NPs had minimal uptake. On T1 imaging, targeted NPs increased CNR by 52.5% which was significantly great than Fc-NPs (CNR increased 17.2%) and non-targeted NPs (CNR increased 18.7%) (p=0.001). Confocal fluorescent microscopy showed that NPs target resident macrophages while the untargeted NPs and Fc-NPs are found diffusely throughout the plaque. Targeted NPs had a greater signal intensity increase in the fibrous cap compared with ($p<0.001$) while non-targeted NPs and Fc-NPs had a greater increase in the lipid core ($p<0.01$).

**Conclusion—**Macrophage-specific (CD36) NPs bind human macrophages and improved MR detection and characterization of human aortic atherosclerosis. Thus, macrophage-specific NPs could help identify high-risk human plaque prior to the development of an atherothrombotic event.

### Keywords

Macrophage; Atherosclerosis; Magnetic resonance imaging; nanoparticles; CD36

## Introduction

The clinical manifestations of atherosclerosis, namely myocardial infarction and stroke, remain the leading cause of morbidity and mortality in the United States(1) and Western society. Since the majority of acute coronary syndromes occur from rupture of lesions less than 50% stenosed (2,3), identification of high-risk lesions in individuals prior to rupture can be challenging. Detection of these lesions by conventional means of assessing atherosclerosis, such as coronary angiography, remains limited(4). Atherosclerotic lesions prone to rupture were shown to have a thin fibrous cap, a large lipid core, and have a large number of inflammatory cells including macrophage-derived foam cells(5,6). Therefore, development of non-invasive imaging agents that target components of atherosclerotic plaque may enable improved detection and characterization of plaque(7).

In an effort to create magnetic resonance imaging (MRI) contrast agents that deliver a large payload of paramagnetic particles, we developed gadolinium (Gd)-loaded lipid-based nanoparticles (NPs) that can be modified to target biological ligands. As previously described, Gd-loaded NPs modified with antibodies targeting macrophage scavenger receptor A (MSR-A or CD204) not only improved *in vitro* MR detection of macrophages but also improved *ex vivo* detection of murine atherosclerosis and macrophage density(8). Recently, NPs targeting the MSR-A were shown to improve in vivo detection of murine atherosclerosis with a high correlation between the signal intensity on MRI and the number of macrophages in the region of interest(9). CD36, a class B scavenger receptor, has been shown to have an important role in oxidized lipoprotein uptake, explaining its increased expression in atherosclerosis. Therefore, we set out to determine whether Gd-labeled NPs targeting CD36 bind to macrophages and improve MR detection and characterization of human atherosclerosis.

## Methods

### Nanoparticles Formulation

The nanoparticles were made from phospholipids [Palmitoyl-oleoyl phosphatidylcholine (POPC), 1,2-Dipalmitoyl-sn-glycero-3-phosphoethanolamine-N-7-nitro-2-1,3-benzoxadiazol-4-yl (DPPE-NBD), 1,2-Dipalmitoyl-sn-glycero-3-phosphoethanolamine-N-biotinyl (DPPE-Biotin)], a surfactant (Tween 80), and an aliphatic gadolinium complex (Gd-DOTA-BSA, Gateway Chemical) as previously described(8,10). POPC and the gadolinium complex were dissolved in a 1:1 chloroform:methanol solution (5mL). Evaporation under

nitrogen flux yielded a thin film that was then rehydrated in hot water (2mL, 70°C). This solution was sonicated for 15 minutes at 70W at 90 % cycle duty while the temperature was kept at 65°C with a thermostatic bath. After sonication, Tween 80 was added, followed by another 15 minutes of sonication. Green fluorescent NBD-labeled untargeted NPs were obtained by adding 2 moles % of fluorescent phospholipid DPPE-NBD to the formulation and red fluorescent rhodamine-labeled untargeted NPs were obtained by adding 2 moles % of fluorescent phospholipid DPPE-rhodamine to the formulation. Biotinylated NPs were prepared by addition of 0.5 moles % of DPPE-Biotin to the reaction mixture. Biotinylated rabbit anti-human polyclonal antibodies to human CD36 (IgG, Novus Biologicals) and biotinylated ChromPure rabbit IgG, Fc fragment (Jackson Immunoresearch) were used to make targeted NPs s and Fc-NPs respectively. Targeted NPs and Fc-NPs were prepared by adding approximately $1.9 \times 10^{-10}$ moles of biotinylated NPs dissolved in phosphate buffered solution (PBS) to $9.7 \times 10^{-10}$ moles of streptavidin (Sigma-Aldrich) and the vial was shaken for 30 minutes. Then $2.3 \times 10^{-9}$ moles of biotinylated anti-CD36 or Fc fragment dissolved in PBS were added to the vial and shaken for another 3.5 hours. This enabled the antibody to bind to the nanoparticle via a biotin-streptavidin-biotin bridge. The solution containing targeted NPs and Fc-NPs therefore had a ratio of 10 parts anti-CD36 or Fc-portion to 5 parts streptavidin to one part nanoparticle, ensuring that excess antibody is available for each particle.

The NPs were characterized by photon correlation spectroscopy performed with a Malvern multiangle dynamic laser light scattering system at room temperature, and inductively coupled plasma-mass spectrometry (ICP-MS) measurements provided the number of Gd ions per particle(11). The relaxivity of contrast agents was determined at 37°C using a 1.5 T clinical scanner. Two formulations of nanoparticles were created for this study.

### In Vitro Protocol

Human peripheral blood THP-1 monocytes were isolated using well established adhesion methods(12). The monocytes were activated by incubation with human recombinant macrophage colony-stimulating factor (1 ug/ml, Sigma). The activated monocytes/ macrophages were plated for one week in Dulbecco's modified Eagle medium (DMEM) containing fetal calf serum. The cells were washed and further activated by the addition of oxidized low density lipoprotein (5 ug/ml, MDA-LDL), as previously described(13). Twenty four hours after the addition of MDA-LDL the cells were washed with fresh culture medium and the nanoparticles added at a concentration of 1 mM Gd. In order to evaluate the competition between the targeted and untargeted particles, cells were incubated as follows: (1) cells incubated with 1 mM Gd of NBD labeled untargeted particles, (2) cells incubated with 1 mM Gd rhodamine labeled targeted particles (CD36), (3) cells incubated with 1 mM Gd NBD labeled untargeted particles and 1 mM Gd rhodamine labeled targeted particles (Cd36), and (4) control cells. All cells were then incubated for 24 hours at 37°C. After incubation, the cells were washed (3×) with PBS and scraped in 0.25 ml of PBS. We then transferred 5 μl of the cell suspension to a slide and smeared using blood smearing techniques. The cells were fixed to the slide (4% para formaldehyde) and washed with PBS. We added 5 μl of DAPI and the slides were mounted and confocal microscopy was performed with 24 hours. The remaining 0.245 ml of cells were measured for cell number (bright light counting chamber) and sent for ICP-MS for Gd quantification. The resultant Gd concentrations (μg/ml) were then normalized to the cell numbers present.

### *Ex Vivo* Protocol

Aortas with moderate to severe atherosclerotic disease were harvested from subjects at the time of autopsy. Each piece of aorta was divided into three equal sections using transverse cuts across the arterial lumen, preserving the lumen and vascular wall. Each section had an approximate height of 1 cm. For this experiment, 16 sections of aorta were selected from a

total of 6 different subjects (4 different aortas yielding 3 sections each and 2 different aortas yielding 2 sections each). The experimental design was for 6 aorta sections to be incubated with CD36 labeled nanoparticles 6 aorta sections to be incubated with untargeted particles, and 4 aorta sections to be incubated with unspecific Fc-particles. Prior to imaging, the sections of aorta were removed from formalin, cleaned, dabbed dry, and placed in Fomblin solution (perfluoropolyether; Ausimont USA Inc.) for MRI. Fomblin does not have a residual MR signal and does not interfere with the biological tissue signal(14). Following the initial pre-contrast MRI, the aorta sections were removed, dabbed dry, placed in individual plastic containers with PBS, and either the solution of targeted NPs, untargeted NPs, or Fc-NPs was added. The plastic containers were covered and placed on a shaker for incubation at 4°C for 24 hours. Following incubation, the aorta sections were removed from the solution, cleaned, dabbed dry, placed in fomblin in their original positions from the pre-contrast imaging, and were imaged.

### *Ex Vivo* Imaging

Pre-contrast and post-contrast imaging of the aorta sections was performed using a Siemens Sonata 1.5 T MR system. Sixteen contiguous axial images were obtained with T1, T2, and proton density weighted spin echo sequences. This enabled 3-dimensional multicontrast analysis of the aortas. T1 images were obtained with a repetition time of 300 ms and an echo time of 9 ms, T2 images were obtained with a repetition time of 2000 ms and an echo time of 55 ms, and proton density weighted images were obtained with a repetition time of 2000 ms and an echo time of 9 ms. The images had a slice thickness of 0.5 mm, matrix size of 512 × 512 pixels, field of view of 12.8 × 12.8 cm, and a resolution of 0.25 × 0.25 mm. T1 sequence acquisition time was 9 minutes, T2 acquisition time was 15 minutes, and PDW sequence acquisition time was less than 15 minutes. The receiver gain was automatically calculated by the MRI system.

### Confocal Fluorescent Microscopy

Confocal laser scanning microscopy was performed at the MSSM-Microscopy Shared Resource Facility using the appropriate light sources and filter sets on the control aortas and aortas incubated with fluorescent CD36 labeled, untargeted and unspecific particles. All arteries were washed and frozen in optical cutting temperature compound (OCT Compound), (Tissue Tek, Sakura Finetech). Ten microns sections were cut and mounted on slides and stained with phycoerythrin (RPE)-labeled anti-CD68 (excitation wavelength: 532 - 561nm, emission wavelength: 578 - 610nm) and 4',6'-diamidino-2-phenylindole hydrochloride (DAPI) (excitation wavelength: 385 - 400nm, emission wavelength: > 450nm). Anti-CD68 is an antibody directed against lysosomal glycoproteins of macrophages(15) while DAPI is known to bind DNA in cellular nuclei(16). The NBD-labeled untargeted NPs had an excitation wavelength of 460nm and emission wavelength of 534nm. Light microscopy was performed with and without hematoxylin and eosin staining to allow histopathological comparison with corresponding MR images.

### Image Analysis

Three-dimensional T1 image analysis was performed for each aorta. Sixteen contiguous slices were obtained and analysis was performed on contiguous slices in which there was no disruption of the aortic wall (the aorta was present as a complete circle). Eight regions of interest spanning the intima, media, and adventitia of equal size in each aorta for pre-contrast slices were selected and the corresponding regions of interest were selected for the corresponding post-contrast slice. The mean signal intensity for the eight regions of interest was calculated for each slice along with the signal intensity of the noise and the standard deviation (SD) of the noise. The signal-to-noise ratio was calculated by the following equation:

$$\text{SNR} = \text{mean signal intensity of 8 regions of interest} / \text{SD of the noise} \quad \text{Equation 1}$$

The mean pre- and post-contrast SNR of each aorta was then determined by taking the average of the SNR for each slice for pre- and post-contrast images respectively. The change in pre- and post-contrast SNR, also known as contrast to noise ratio (CNR), was determined by the following equation:

$$\text{CNR} = ((\text{Post-Con SNR} - \text{Pre-Con SNR}) / \text{Pre-Con SNR}) \times 100 \quad \text{Equation 2}$$

Composition images were created by merging red, green, and blue images in which the T1 image was converted to a red image, T2 was converted to a green image, and PDW was converted to a blue image(14). The histopathological section for each aorta was then compared with the matching composition image. Type IV and Type V lesions as defined by Stary and colleagues(17) were identified on histopathological images. A dense accumulation of extracellular lipid that occupies an extensive but well-defined region of the intima was used to define a lipid core(17). The tissue layer between the lipid core and the endothelial surface was defined as the fibrous cap(17). Cluster analysis was performed by determining the T1 pre-contrast and post-contrast SNR for each aorta in regions of lipid core and fibrous cap.

### Statistical Analysis

Comparison of SNR between pre- and post-contrast T1 images was performed using paired student T-test analysis. One-way analysis of variance (ANOVA) was performed to compare between treatment groups for pre-contrast SNR and post-contrast SNR respectively. Two-way ANOVA was performed to compare the CNR of particular imaging agents to determine superiority of one agent compared with another. Pair-wise comparisons were made without adjustment for Type I error rates. Results are shown as mean ± standard deviation (SD). P-values less than 0.05 were considered significant. Number Crunching System Software (Salt Lake City, Utah) was used for all statistical analyses.

## Results

Two formulations of nanoparticles were created for this study. The first formulation was a biotinylated particle with the following characteristics: average of 14,900 Gd atoms per nanoparticle, average diameter of 125.2 nm, and an average relaxivity of 37.1 $mM^{-1}s^{-1}$. The second formulation included fluorescent NBD-labeled or rhodamine-labeled biotinylated particle with the following characteristics: average of 13,800 Gd atoms per nanoparticle, average diameter of 125.2 nm, and an average relaxivity of 36.0 $mM^{-1}s^{-1}$.

Activated human monocytes were incubated for 24 hours at 37°C with control media, NBD-labeled (green) untargeted particles (1 mM Gd), rhodamine-labeled (red) anti-CD36 particles (1 mM Gd), and a combination of untargeted and targeted particles (2 mM Gd). Cells were then prepared for confocal microscopy and the remaining cells were counted and sent to ICP-MS for determination of Gd concentrations with normalization for cell number. As seen in Figure 1, there is clear uptake of the red rhodamine-labeled anti-CD36 particles by activated lipid rich human monocyte derived macrophages as demonstrated by both confocal microscopy and ICP-MS Gd quantification. As shown, there was only limited uptake of NBD-labeled untargeted particle.

Mean SNR values for pre- and post-contrast T1 images are presented in Table 1 for each aorta section grouped according to whether incubated with untargeted, CD36 labeled and unspecific-

Fc particles. ANOVA demonstrated no significant difference between mean SNR of aorta groups prior to incubation with contrast agents (Table 1). Pre- and post-contrast T1 analysis demonstrated that targeted NPs, increased CNR by 52.5% (20.3±1.8 vs 30.9±3.0, $p<0.0001$) while Fc-particles increased CNR by 17.2% (20.7±1.0 vs 24.2±0.6, $p<0.0001$) and untargeted particles increased CNR by 18.7% (21.7±1.3 vs 25.7±1.3, $p<0.0001$). Matched pre- and post-contrast MR images of aortas treated with untargeted, CD36 labeled and unspecific-Fc particles can be seen in Figure 2 and illustrates the greater increase in signal intensity seen with CD36 labeled particles relative to the untargeted and unspecific particle formulations. CD36 labeled particles increased CNR significantly greater when compared with Fc-NPs (F-Ratio 33.8, $p<0.0003$) or when compared with the untargeted analogue (F-Ratio 45.0, $p<0.0001$) on 2-way ANOVA. However, the CNR was not significantly different between aortas treated with untargeted and unspecific-Fc particles (F-Ratio 2.25, $p=0.18$).

Confocal fluorescence microscopy was performed on aortas incubated in NBD-labeled untargeted, CD36 labeled and unspecific-Fc particles. As shown in Figure 3, red-fluorescent RPE-labeled anti-CD68, an antibody proven to specifically target macrophage lysosomes (15), co-localizes with green fluorescent NBD-labeled targeted particles in the plaque. Since the macrophages are no longer viable, the colocalization likely represents binding of targeted NPs to CD36 expressed on the surface of resident macrophages in the atherosclerotic plaque. A corresponding light microscopic image reveals that the resident macrophages are heavily present in a small atheroma with a thin fibrous cap. Figure 4 demonstrates confocal microscopy of aortic atherosclerotic plaques treated with untargeted and unspecific-Fc NPs. It demonstrates non-specific distribution of these formulations within the aortic plaque. While there is non-specific distribution in the atherosclerotic plaque with CD36 labeled particles, there is significant binding to macrophages as previously shown. The control aorta demonstrates nuclear staining with DAPI and the staining of macrophages with red-fluorescent RPE-labeled anti-CD68.

Cluster analysis was performed by measuring SNR on pre- and post-contrast T1 images in the lipid core or fibrous cap based on comparison of composition images with histopathological images stained with hematoxylin and eosin. Image comparison can be seen in Figure 5. Pre- and post-contrast SNR data for fibrous cap and lipid core are available in Table 2. Two-way ANOVA demonstrated that there was a greater increase in SNR in the fibrous cap compared with the lipid core following incubation with CD36 labeled NPs (75.2% vs 43.7% respectively, $p<0.0003$). However, there was a greater increase of SNR in the lipid core compared with the fibrous cap following incubation with untargeted (24.7% vs 16.9% respectively, $p<0.0001$) and unspecific-Fc particles (22.5% vs 15.1% respectively, $p<0.01$). Aortic plaque incubated with the CD36 labeled particles appeared to have the greatest increase in signal intensity in regions with a large number of resident macrophages bound by NBD-labeled targeted NPs (Figure 3).

## Discussion

The findings of this study demonstrate that Gd-loaded nanoparticles targeting CD36, a class B scavenger receptor, were able to specifically target human macrophages in vitro as demonstrated by confocal microscopy and ICP-MS. Anti-CD36 NPs had significantly greater CNR in cadaveric human aortic atherosclerosis than untargeted and unspecific-Fc particles on T1 MR images. Additionally, fluorescent confocal microscopy validated that NBD-labeled Cd36 labeled particles targeted resident macrophages through colocalization of NBD-labeled targeted NPs and RPE-labeled anti-CD68. While untargeted and unspecific-Fc particles were shown to be non-specifically distributed throughout the atherosclerotic plaque on confocal microscopy, the CD36 labeled particles both specifically targeted the macrophages and were also non-specifically distributed throughout the plaque. Finally, this study demonstrates that

that the CD36 labeled particles had a greater CNR on T1 images in fibrous plaque while untargeted and unspecific-Fc particles had a greater CNR on T1 images in lipid-rich plaque. The greatest increase in the fibrous plaque with CD36 targeted particles appeared to occur on periphery of the lipid-rich plaque through binding to macrophages surrounding the lipid-rich core.

Targeted imaging of macrophages as a possible means of detecting and characterizing atherosclerosis has been investigated using multiple imaging modalities(18). The use of CD36 labeled particles that specifically target the macrophage scavenger receptor to detect atherosclerosis using MRI was previously investigated in a murine model of atherosclerosis (8,9). The targeted NPs were shown to specifically target CD204 (macrophage scavenger receptor types I & II) and resulted in increased binding and uptake in murine macrophages (8). Incubation of cells with oxidized low density lipoprotein and excess anti-CD204 were both shown to reduce binding of targetedz NPs s targeting CD-204(8). Additionally, ex vivo imaging of murine aortic atherosclerosis following incubation with contrast agents(8) and in vivo aortic plaque MR imaging in mice injected with contrast agent(9) revealed that greater enhancement of the atherosclerotic plaque occurs with targeted NPs compared with non-targeted NPs and targeted NPs specifically bound resident macrophages in the plaque. In the current study, we employed rabbit anti-human antibodies targeting CD36, a member of the class B scavenger receptor family. Both CD36 and MSR-A have been shown to play a role in the development of atherosclerosis and collectively are responsible for binding and uptake of 75 to 90% of modified low density lipoprotein uptake by macrophages(19). Several studies have highlighted the importance of CD36 for plaque development by demonstrating significant reduction in the short-term and long-term development of atherosclerosis in mice with Apo-E knockout and CD36 knockout compared with Apo-E knockout mice(20,21). Additionally, transplantation of stem cells with CD36 in the double knockout mice (CD36 -/-, Apo-E -/-) resulted in increased development of atherosclerosis(22). However, Moore and colleagues(23) found that Apo-E knockout mice lacking CD36 had greater aortic sinus atherosclerosis development than Apo-E knockout mice. This study demonstrates the potential to use molecular MR imaging with NPs targeting CD36 to improve the detection and characterization of atherosclerotic plaque and may serve as a way to investigate the role of CD36 in the progression or regression of atherosclerosis.

Detection of atherosclerosis using MRI has also been achieved using superparamagnetic iron oxide particles (SPIOs). While studies have demonstrated that SPIOs are taken up by macrophages in atherosclerotic plaque, a recent study investigated the mechanism of cellular uptake of SPIOs. von Zur Muhlen and colleagues(24) demonstrated that the integrin Mac-1 is crucial in the uptake of SPIOs and binding/uptake was significantly reduced after blocking Mac-1 with antibodies targeting CD11b. Ultrasmall SPIOs have been shown to detect inflamed carotid atherosclerotic plaques with correlation to macrophage density(25). Additionally, echogenic imaging agents could be developed to target macrophages in atherosclerotic plaque and enhance plaque detection and characterization. Nuclear imaging with positron emission tomography and single photon emission computed tomography with imaging agents taken up by macrophages and foam cells may enable detection and characterization of inflamed atherosclerotic plaque(26). Finally, targeted imaging of macrophages with contrast agents for computed tomography(27), optical imaging, or with multimodal imaging agents(28) seems very promising.

One limitation of this study is that the imaging was not performed on viable aorta due to the ex vivo study design in which the aorta was harvested at the time of autopsy from human subjects. However, our data does demonstrate uptake of targeted and untargeted NPs by human macrophages in vitro. Additionally, we did not determine the role particle diffusion played in our study and whether there was greater binding at the surface compared with more central or

deep macrophages. Staining for MSR-A would have provided additional information regarding the expression of other scavenger receptors on the surface of macrophages in the aortic atherosclerotic plaque and enable comparison with prior studies that investigated scavenger receptor expression(29). Another limitation in the use of particles targeting CD36 is that intravenous administration of this imaging agent will suffer first pass effect in the liver by binding to scavenger receptors expressed on the surface of Kuppfer cells(18). Toxicity data for the lipid based particle platform is also lacking, however studies indicate that liver uptake of the gadolinium labeled particles may limit clinical translation(30). Similarly, this study only evaluated colocalization with macrophages and did not assess binding of anti-CD36 targetd particles to other cells that express CD36 such as endothelial cells, smooth muscle cells, adipocytes, and platelets. An additional limitation of this agent in its current form is the use of rabbit antibodies targeting human CD36. These antibodies will likely result in an immune response against the antibody portion of the imaging agent and would therefore limit the use of this agent in tracking progression/regression of atherosclerotic plaque. Future studies should include isotype-matched antibodies to further test specificity of the antibody targeting. Finally, the role of imaging with nanoparticles targeting CD36 remains to be validated for in vivo atherosclerotic plaque detection.

In conclusion, Gd-loaded lipid based nanoparticles targeting CD36, a class B scavenger receptor, had significant uptake by human macrophages in vitro, improved signal intensity of ex vivo aortic atherosclerotic plaque, and were shown to bind to resident macrophages in atherosclerotic plaque on confocal microscopy. Finally, the CD36 label3d particles created the largest signal intensity in regions of fibrous plaque on the periphery of lipid-rich plaque. These data suggest that lipid based nanoparticles targeting CD36 may improve detection and characterization of atherosclerotic plaque and determine the degree of plaque inflammation by assessing macrophage density.

## Acknowledgments

This study was supported in part by NIH/NHLBI ROI HL71021, NIH/NHLBI HL078667 (ZAF), and the Stanley J. Sarnoff Endowment for Cardiovascular Research, Inc. (V.A.). The MSSM-Microscopy Shared Resource Facility is supported by funding from NIH-NCI shared resources grant R24 CA095823, and NSF Major Research Instrumentation grant DBI-9724504.

## References

1. Heart Disease and Stroke Statistics-2006 Update. The American Heart Association; Dallas, TX: 2006.
2. Ambrose JA, Tannenbaum MA, Alexopoulos D, et al. Angiographic progression of coronary artery disease and the development of myocardial infarction. J Am Coll Cardiol 1988;12:56–62. [PubMed: 3379219]
3. Little WC, Constantinescu M, Applegate RJ, et al. Can coronary angiography predict the site of a subsequent myocardial infarction in patients with mild-to-moderate coronary artery disease? Circulation 1988;78:1157–66. [PubMed: 3180375]
4. Topol EJ, Nissen SE. Our preoccupation with coronary luminology. The dissociation between clinical and angiographic findings in ischemic heart disease. Circulation 1995;92:2333–42. [PubMed: 7554219]
5. Davies MJ, Richardson PD, Woolf N, Katz DR, Mann J. Risk of thrombosis in human atherosclerotic plaques: role of extracellular lipid, macrophage, and smooth muscle cell content. Br Heart J 1993;69:377–81. [PubMed: 8518056]
6. Carr S, Farb A, Pearce WH, Virmani R, Yao JS. Atherosclerotic plaque rupture in symptomatic carotid artery stenosis. J Vasc Surg 1996;23:755–65. [PubMed: 8667496]discussion 765-6
7. Lipinski MJ, Fuster V, Fisher EA, Fayad ZA. Technology Insight: targeting of biological molecules for evaluation of high-risk atherosclerotic plaques with magnetic resonance imaging. Nat Clin Pract Cardiovasc Med 2004;1:48–55. [PubMed: 16265260]

8. Lipinski MJ, Amirbekian V, Frias JC, et al. MRI to detect atherosclerosis with gadolinium-containing immunomicelles targeting the macrophage scavenger receptor. Magn Reson Med 2006;56:601–10. [PubMed: 16902977]
9. Amirbekian V, Lipinski MJ, Briley-Saebo KC, et al. Detecting and assessing macrophages in vivo to evaluate atherosclerosis noninvasively using molecular MRI. Proc Natl Acad Sci U S A 2007;104:961–6. [PubMed: 17215360]
10. Kimpe K, Parac-Vogt TN, Laurent S, et al. Potential MRI Contrast Agents Based on Micellar Incorporation of Amphiphilic Bis(alkylamide) Derivatives of [(Gd-DTPA)(H2O)]2- Eur J Inorg Chem 2003;2003(16):3021–3027.
11. Winter PM, Caruthers SD, Yu X, et al. Improved molecular imaging contrast agent for detection of human thrombus. Magn Reson Med 2003;50:411–6. [PubMed: 12876719]
12. Bannon PG, Dean RT, Dawes J. Isolation and maintenance of nonadherent quiescent human monocytes for studies of adhesion and migration. Methods in Cell Science 1995;17:53–59.
13. Briley-Saebo KC, Shaw PX, Mulder WJ, et al. Targeted molecular probes for imaging atherosclerotic lesions with magnetic resonance using antibodies that recognize oxidation-specific epitopes. Circulation 2008;117:3206–15. [PubMed: 18541740]
14. Itskovich VV, Samber DD, Mani V, et al. Quantification of human atherosclerotic plaques using spatially enhanced cluster analysis of multicontrast-weighted magnetic resonance images. Magn Reson Med 2004;52:515–23. [PubMed: 15334569]
15. Holness CL, Simmons DL. Molecular cloning of CD68, a human macrophage marker related to lysosomal glycoproteins. Blood 1993;81:1607–13. [PubMed: 7680921]
16. Hajduk SL. Demonstration of kinetoplast DNA in dyskinetoplastic strains of Trypanosoma equiperdum. Science 1976;191:858–9. [PubMed: 1251198]
17. Stary HC, Chandler AB, Dinsmore RE, et al. A definition of advanced types of atherosclerotic lesions and a histological classification of atherosclerosis. A report from the Committee on Vascular Lesions of the Council on Arteriosclerosis, American Heart Association. Arterioscler Thromb Vasc Biol 1995;15:1512–31. [PubMed: 7670967]
18. Lipinski MJ, Frias JC, Fayad ZA. Advances in detection and characterization of atherosclerosis using contrast agents targeting the macrophage. J Nucl Cardiol 2006;13:699–709. [PubMed: 16945750]
19. Kunjathoor VV, Febbraio M, Podrez EA, et al. Scavenger receptors class A-I/II and CD36 are the principal receptors responsible for the uptake of modified low density lipoprotein leading to lipid loading in macrophages. J Biol Chem 2002;277:49982–8. [PubMed: 12376530]
20. Guy E, Kuchibhotla S, Silverstein R, Febbraio M. Continued inhibition of atherosclerotic lesion development in long term Western diet fed CD36o /apoEo mice. Atherosclerosis 2007;192:123–30. [PubMed: 16919281]
21. Febbraio M, Podrez EA, Smith JD, et al. Targeted disruption of the class B scavenger receptor CD36 protects against atherosclerotic lesion development in mice. J. Clin. Invest 2000;105:1049–1056. [PubMed: 10772649]
22. Febbraio M, Guy E, Silverstein RL. Stem cell transplantation reveals that absence of macrophage CD36 is protective against atherosclerosis. Arterioscler Thromb Vasc Biol 2004;24:2333–8. [PubMed: 15486305]
23. Moore KJ, Kunjathoor VV, Koehn SL, et al. Loss of receptor-mediated lipid uptake via scavenger receptor A or CD36 pathways does not ameliorate atherosclerosis in hyperlipidemic mice. J Clin Invest 2005;115:2192–201. [PubMed: 16075060]
24. von Zur Muhlen C, von Elverfeldt D, Bassler N, et al. Superparamagnetic iron oxide binding and uptake as imaged by magnetic resonance is mediated by the integrin receptor Mac-1 (CD11b/CD18): Implications on imaging of atherosclerotic plaques. Atherosclerosis 2006;193:102–11. [PubMed: 16997307]
25. Trivedi RA, Mallawarachi C, JM UK-I, et al. Identifying Inflamed Carotid Plaques Using In Vivo USPIO-Enhanced MR Imaging to Label Plaque Macrophages. Arterioscler Thromb Vasc Biol. 2006
26. Davies JR, Rudd JH, Weissberg PL, Narula J. Radionuclide imaging for the detection of inflammation in vulnerable plaques. J Am Coll Cardiol 2006;47:C57–68. [PubMed: 16631511]
27. Hyafil F, Cornily JC, Feig JE, et al. Noninvasive detection of macrophages using a nanoparticulate contrast agent for computed tomography. Nat Med 2007;13:636–41. [PubMed: 17417649]

28. Sosnovik DE, Nahrendorf M, Deliolanis N, et al. Fluorescence tomography and magnetic resonance imaging of myocardial macrophage infiltration in infarcted myocardium in vivo. Circulation 2007;115:1384–91. [PubMed: 17339546]

29. Nakata A, Nakagawa Y, Nishida M, et al. CD36, a Novel Receptor for Oxidized Low-Density Lipoproteins, Is Highly Expressed on Lipid-Laden Macrophages in Human Atherosclerotic Aorta. Arterioscler Thromb Vasc Biol 1999;19:1333–1339. [PubMed: 10323787]

30. Briley-Saebo KC, Amirbekian V, Mani V, et al. Gadolinium mixed-micelles: effect of the amphiphile on in vitro and in vivo efficacy in apolipoprotein E knockout mouse models of atherosclerosis. Magn Reson Med 2006;56:1336–46. [PubMed: 17089381]

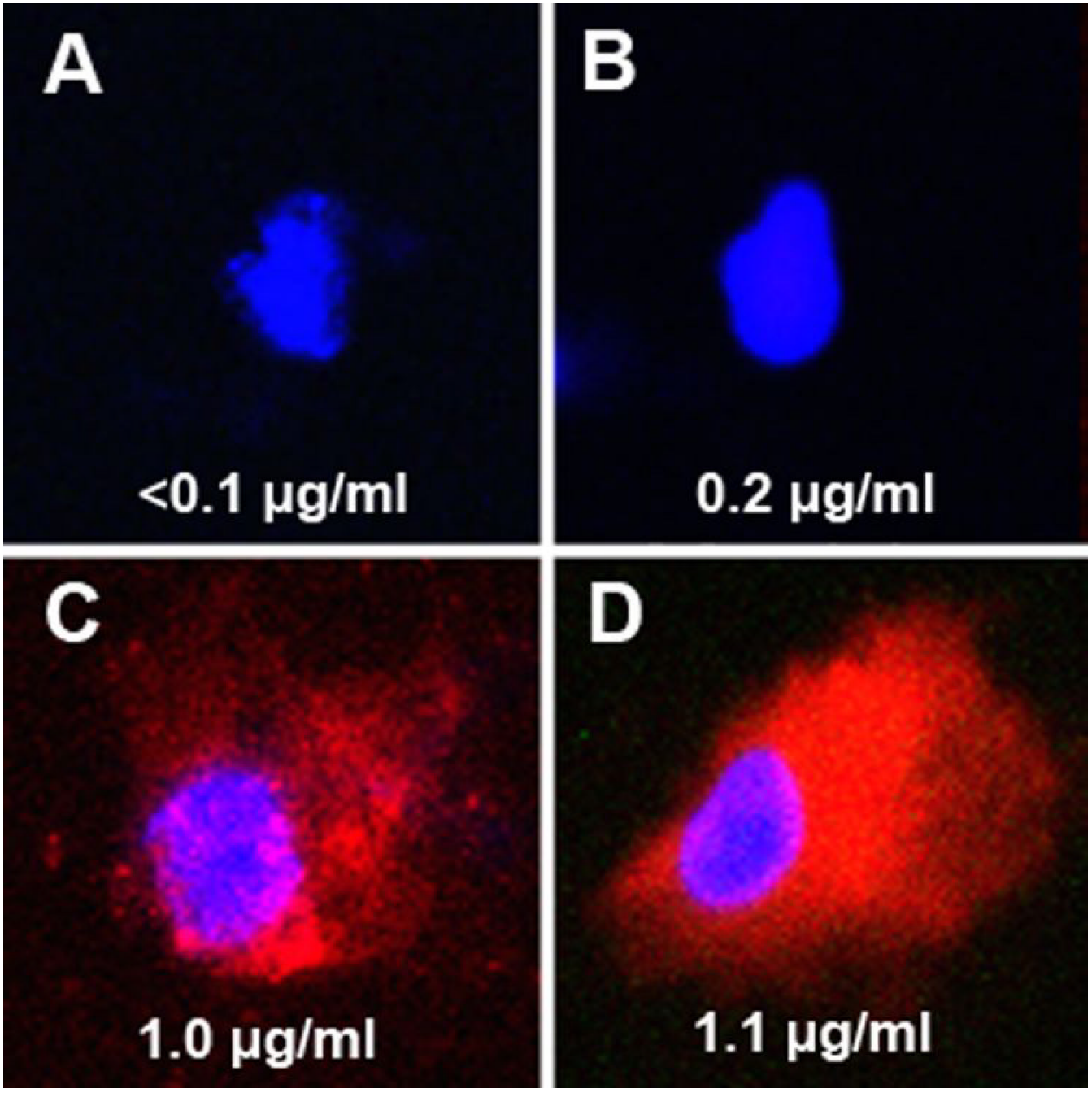


**Figure 1. Confocal microscopy demonstrating in vitro macrophage uptake of NPs**

Confocal microscopy merged images (NBD=green, rhodamine=red, DAPI=blue) at 100X of activated human monocytes incubated in vitro with control (A), NBD-labeled untargeted NPs (B), rhodamine-labeled NPs targeting CD36 (C), and with both NBD-labeled untargeted NPs and rhodamine-labeled NPs targeting CD36 (D) and stained with DAPI. Included with each image in the bottom of the panel is the Gd concentration (µg/ml) normalized to the cell numbers present. As seen in panel A, the nuclei of the control cells appear blue and there was no significant GD present as expected. In cells incubated with untargeted NBD-labeled NPs (B), there was trivial green fluorescence seen and minimal uptake of Gd as seen on ICP-MS. Cells incubated with rhodamine-labeled NPs targeting C36 (C) demonstrated significant red

fluorescence corresponding with cellular uptake of targeted NPs and ICP-MS also demonstrated significant Gd uptake. As seen in Panel D, there was again significant uptake of rhodamine-labeled NPs targeting CD36 but trivial uptake of untargeted NBD-labeled NPs. The cellular uptake of Gd as shown on ICP-MS in panel D appears similar to the sum of Gd concentrations for panels B and C.

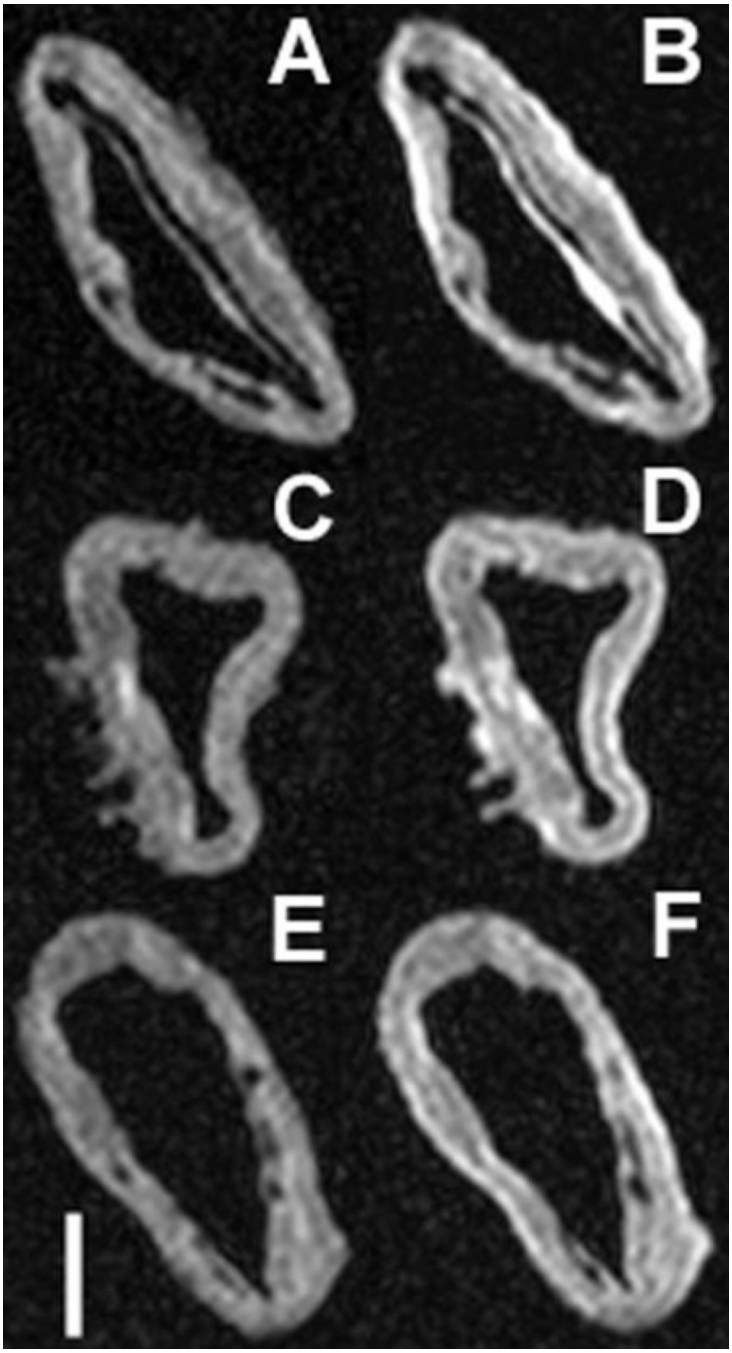


**Figure 2. Pre- and post-contrast MRI of aorta incubated with NPs**

Comparison of pre- and post-contrast T1 images of aortas treated with Gd-loaded NPs targeting CD36 (A & B respectively), untargeted NPs (C & D respectively), and Fc-NPs (E & F respectively). Included in the bottom left corner is a scale bar that represents one centimeter in length. The error bar graph included below (Figure 2B) provides a graphical representation comparing preand post-contrast SNR seen between aorta sections incubated with targeted NPs, untargeted NPs, and Fc-NPs.

A

B

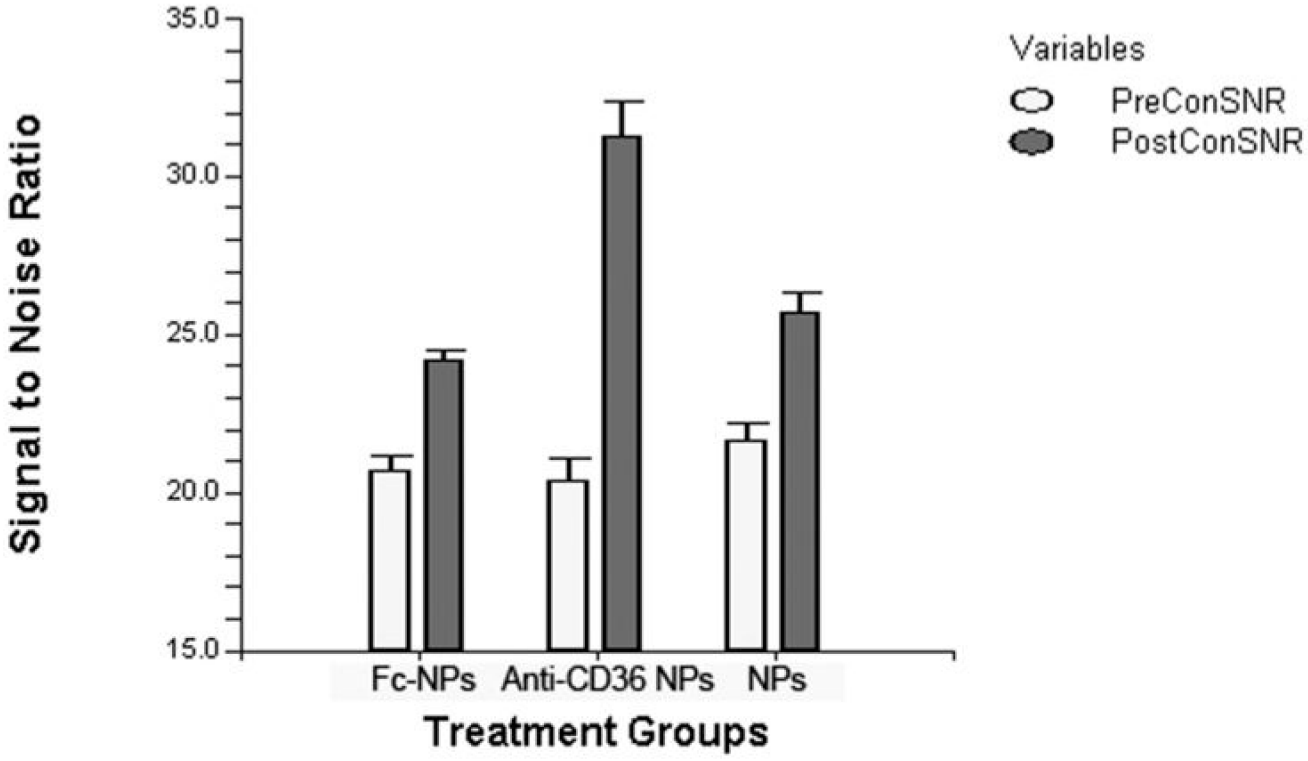


**Figure 3. Confocal microscopy of atherosclerotic plaque demonstrating fluorescent macrophage-specific NPs**

Confocal microscopy images of aortic atherosclerotic plaque incubated with (A) NBD-labeled (green) NPs targeting CD36, (B) DAPI (blue), (C) RPE-labeled (red) anti-CD68 (macrophage lysosomes). The merged image (D) demonstrates co-localization of NDB-labeled NPs targeting CD36 (macrophage scavenger receptor) and RPE-labeled anti-CD68. The arrow points to an atheroma with high macrophage content and thin fibrous cap. (E) Corresponding light microscope image.

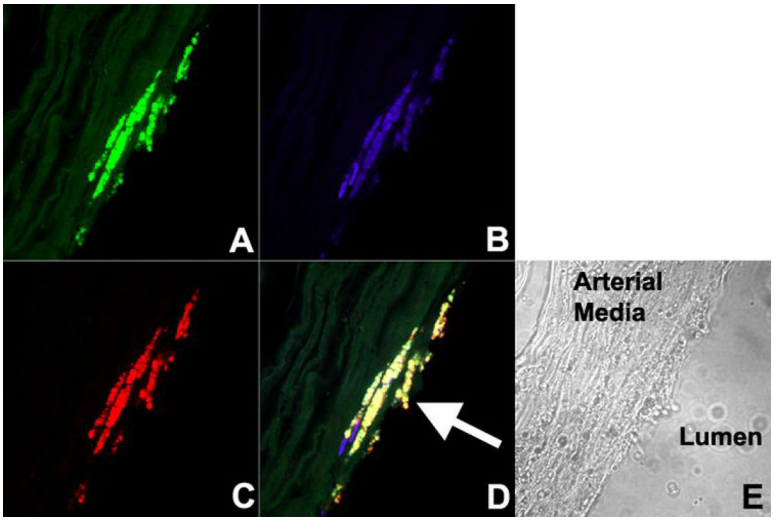


**Figure 4. Confocal microscopy of plaque demonstrating uptake of NPs**

Confocal microscopy merged images (NBD=green, anti-CD68=red, DAPI=blue) at 100X of atherosclerotic plaque incubated with (A) control (non-fluorescent untargeted NPs), (B) NBD-labeled untargeted NPs, (C) NBD-labeled Fc-NPs, (D) and NBD-labeled targeted NPs. The images were of the intimal plaque and therefore do not have the auto-fluorescence of the internal elastic lamina and media. There was no green fluorescence seen in control aortic plaque incubated with non-fluorescent untargeted NPs while non-specific distribution of NBD-labeled untargeted NPs, Fc-NPs, and targeted NPs can be seen throughout the plaque. An arrow is present in each image to identify resident macrophages. Significant colocalization was seen of NBD-labeled targeted NPs and anti-CD68 (D) while significant colocalization was not seen with NBD-labeled untargeted NPs and Fc-NPs (B & C). This suggests that macrophages are bound by targeted NPs targeting CD36.

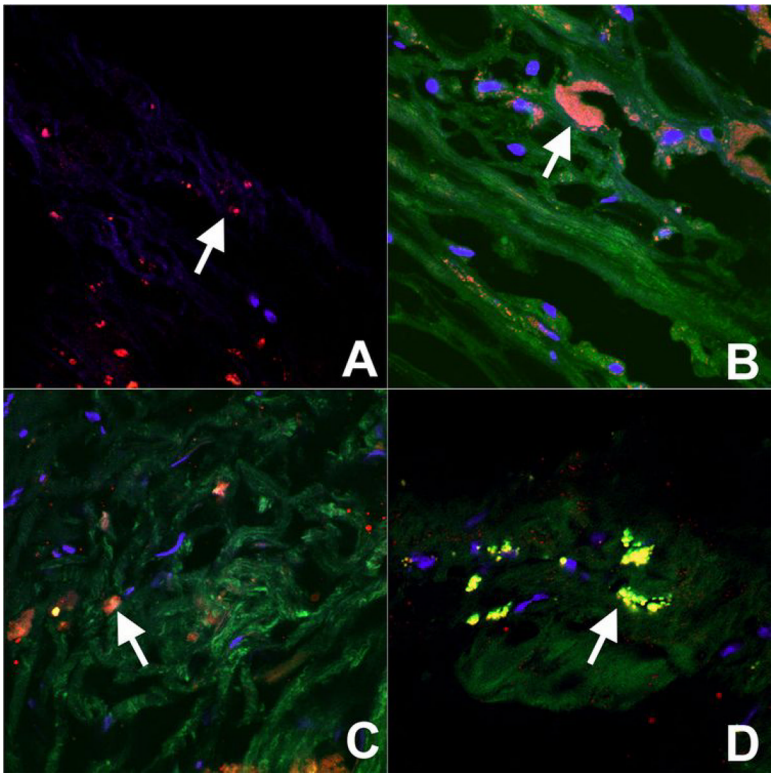


**Figure 5. MRI composition images compared with histopathology of aortic plaque**

The top image is a composition image created by merging T1 image converted to red, T2 converted to green, and PDW converted to blue. Included in the image is a scale bar that represents one centimeter. Below is a comparison of the composition images with the corresponding light microscope images stained with hematoxylin. Aorta specimens below were incubated for 24 hours with targeted NPs (A), untargeted NPs (B & D), and Fc-NPs (C). Below using histopathological comparison, it is able to determine regions of the plaque such as the lipid-rich core (E), the fibrous cap (F), and heavily calcified regions of the plaque (G). The aorta represented in image D is an example of a heavily calcified aorta consistent with a type Vb classification while aorta specimens in image A, B, and C tend to have numerous type IV and Va lesions.

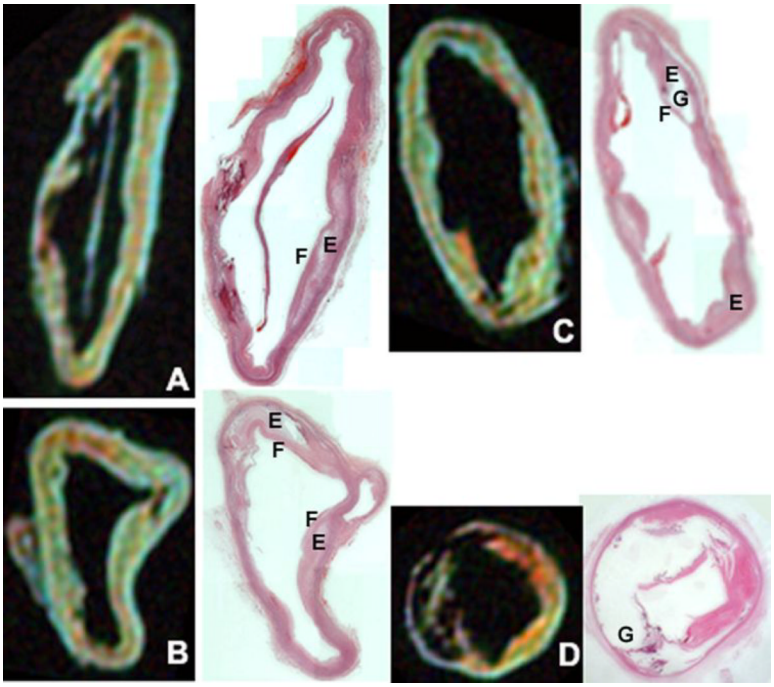


**Figure 6.**

**Table 1**

Pre- and Post-contrast SNR values and CNR values demonstrating the degree of aortic plaque enhancement with Gd-loaded NPs targeting CD36, Fc-NPs, and untargeted NPs. Numbers are expressed as Mean±SD

| Variable | Pre-Con SNR | Post-Con SNR | CNR | Paired T-test | 2-way ANOVA |
|---|---|---|---|---|---|
| **Targeted nanoparticles** | | | | | |
| Aorta 1 | 20.2 ± 2.9 | 32.9 ± 7.3 | | | |
| Aorta 2 | 21.5 ± 0.6 | 31.8 ± 1.0 | | | |
| Aorta 3 | 22.7 ± 0.7 | 33.3 ± 0.5 | | | |
| Aorta 4 | 17.8 ± 0.4 | 26.1 ± 0.4 | | | |
| Aorta 15 | 20.2 ± 0.5 | 31.2 ± 1.0 | | | |
| Aorta 16 | 19.0 ± 0.2 | 28.8 ± 0.1 | | | |
| **Average** | **20.3 ± 1.8** | **30.9 ± 3.0** | **52.5%** | **T-value-15.3, p-value<0.0001** | |
| **Untargeted nanoparticles** | | | | | |
| Aorta 5 | 20.4 ± 2.8 | 24.8 ± 2.8 | | | |
| Aorta 6 | 23.0 ± 0.6 | 27.5 ± 1.6 | | | |
| Aorta 7 | 23.3 ± 0.3 | 26.9 ± 0.2 | | | |
| Aorta 8 | 21.2 ± 0.4 | 24.4 ± 0.6 | | | |
| Aorta 13 | 21.6 ± 0.3 | 25.7 ± 0.6 | | | |
| Aorta 14 | 20.2 ± 0.4 | 24.1 ± 0.6 | | | |
| **Average** | **21.7 ± 1.3** | **25.7 ± 1.3** | **18.7%** | **T-value -14.3, p-value<0.0001** | |
| **Fc-nanoparticles** | | | | | |
| Aorta 9 | 19.9 ± 3.2 | 23.7 ± 3.2 | | | |
| Aorta 10 | 20.6 ± 0.4 | 24.0 ± 0.4 | | | |
| Aorta 11 | 21.5 ± 0.1 | 25.0 ± 0.2 | | | |
| Aorta 12 | 21.2 ± 0.3 | 24.3 ± 0.5 | | | |
| **Average** | **20.7 ± 1.0** | **24.2 ± 0.6** | **17.2%** | **T-value-15.3, p-value<0.0001** | **F-Ratio 16.1, p-value<0.0001** |
| **One-way ANOVA** | **F-Ratio 1.50, p-value 0.26** | **F-Ratio 15.6, p-value <0.0004** | | | |

**Table 2**

Pre- and post-contrast SNR values of the fibrous cap and the lipid core in human aortic atherosclerosis incubated with targeted NPs, untargeted NPs, and Fc-NPs. This table enables determination for each contrast agent of whether CNR is greater in the fibrous cap or the lipid core. Numbers are expressed as Mean±SD

| Variable | Pre-Con SNR | Post-Con SNR | CNR | T-value | p-value |
|---|---|---|---|---|---|
| **Fibrous Cap** | | | | | |
| **Targeted nanoparticles** | 23.8 ± 0.5 | 41.7 ± 1.2 | **75.2%** | -24.3 | <0.0001 |
| **Untargeted nanoparicles** | 23.6 ± 0.5 | 27.6 ± 0.7 | **16.9%** | -28.8 | <0.0001 |
| **Fc-nanoparicles** | 23.9 ± 0.5 | 27.5 ± 0.5 | **15.1%** | -8.9 | <0.001 |
| **Lipid Core** | | | | | |
| Targeted nanoparticles | 16.7 ± 0.8 | 24.0 ± 1.1 | **43.7%** | -19.8 | <0.0001 |
| **Untargeted nanoparicles** | 17.0 ± 0.5 | 21.2 ± 0.5 | **24.7%** | -48.1 | <0.0001 |
| **Fc-nanoparicles** | 16.5 ±0.2 | 20.2 ± 0.6 | **22.5%** | -20.4 | <0.0001 |